

# Optimized Gradient Waveforms for Spiral Scanning

Kevin F. King, Thomas K. F. Foo, Carl R. Crawford

**Spiral scanning gradient waveforms can be optimized with respect to blurring from off-resonance effects by minimizing the readout time. This is achieved by maximizing the gradient amplitude during the scan so that the edge of  $k$ -space is reached as quickly as possible. Gradient hardware constraints are incorporated by considering a circuit model for the gradient coil and amplifier. The optimized gradient waveforms are determined by a set of coupled differential equations. The resulting solutions have shorter readout time than solutions that do not consider the circuit model.**

**Key words: spiral scanning; fast imaging; magnetic resonance imaging.**

## INTRODUCTION

Spiral scanning has been demonstrated for coronary artery imaging (1), abdominal imaging (2), flow imaging (3), and measuring blood oxygen level dependent (BOLD) contrast (4). Advantages of spiral scanning include fewer excitations than conventional Cartesian spin warp methods and lower sensitivity to motion and flow artifacts (5, 6). The main problem with spiral scanning is relatively long readout time compared to Cartesian scanning, which leads to blurring if spins are off resonance due to  $B_0$  inhomogeneity, chemical shift or susceptibility (7–9). The phase accumulated by off-resonant spins increases with time. High frequencies are measured with a greater time delay from the center of  $k$ -space than low frequencies, leading to blurring that increases with readout time. The blurring is significantly worse than the effect of high frequency attenuation due to  $T_2^*$ . Minimizing the blurring may be of greater importance than motion and flow effects for high resolution scanning. Typically, multiple interleaves are used to reduce the blurring by allowing reduced readout time per interleaf while keeping the spatial resolution fixed. For a given spatial resolution, field of view (FOV), and number of interleaves, the blurring is minimized by maximizing the gradient amplitude during the acquisition, because this reduces the time required to reach the edge of  $k$ -space.

In this paper, we focus on 2D spirals, but note that the methods are applicable to 3D spirals (10) as well. Three types of 2D spiral trajectory have been shown: constant angular velocity (11), constant slew rate with negligible acceleration (3), and maximum gradient (1, 12). The advantages of each are as follows. Spirals using the maximum gradient amplitude have the shortest readout time. Spirals with constant slew rate and negligible accelera-

tion have mathematically closed form gradients at large radii in  $k$ -space. Constant angular velocity spirals can be reconstructed with filtered backprojection, avoiding the aliasing artifacts attendant with interpolation (13) or gridding (14), which are required by the other two methods. With reasonable computing power, mathematically closed form gradients are not a major advantage. The aliasing that accompanies gridding can be reduced to an acceptable level by careful choice of reconstruction parameters (15). Therefore, the best approach is to use the maximum gradient.

All spiral techniques must incorporate hardware constraints into calculation of the gradient waveforms. The constraints typically relate to instantaneous peak current, root mean squared (RMS) current and current slew rate for the gradient driver. In this paper, we incorporate the hardware constraints by considering a circuit model for the gradient coil. We show that, with this model, the gradient waveforms are determined by a set of coupled differential equations. The solutions have shorter readout times than solutions which do not consider the circuit model and hence lead to reduced blurring.

## SPIRAL $k$ -SPACE TRAJECTORY

Throughout the paper we use bold font to denote a vector. The Cartesian components ( $k_x, k_y$ ) of the  $k$ -space position  $\mathbf{k}$  can be written in polar coordinates ( $k, \theta$ ) as

$$k_x = k \cos \theta, \quad [1]$$

$$k_y = k \sin \theta. \quad [2]$$

To maximize sampling efficiency, we consider only radially uniform spiral  $k$ -space sampling. It is straightforward to show that radially uniform sampling requires constant  $\frac{dk}{d\theta}$ . Using the convention that  $k = 0$  at  $\theta = 0$ , uniform sampling requires an Archimedean spiral, defined by the requirement that

$$k(t) = A\theta(t), \quad [3]$$

where  $A$  is a constant. The time dependence of  $\theta$  determines the rate of traversal of the spiral trajectory. The purpose of the rest of the paper is to show an algorithm for calculating  $\theta(t)$ .

The value of  $A$  is determined by the Nyquist criterion that

$$\Delta k \leq \frac{M}{D}, \quad [4]$$

where  $\Delta k$  is the radial distance advanced by one interleaf during one rotation,  $D$  is the scan FOV, and  $M$  is the

MRM 34:156–160 (1995)

From G.E. Medical Systems, Milwaukee, Wisconsin and Analogic Corporation, Peabody, Massachusetts (C.R.C.).

Address correspondence to: Kevin F. King, Ph.D., G.E. Medical Systems, P.O. Box 414, W-875, Milwaukee, WI 53201.

Received December 6, 1994; revised April 20, 1995; accepted May 4, 1995.

0740-3194/95 \$3.00

Copyright © 1995 by Williams & Wilkins

All rights of reproduction in any form reserved.

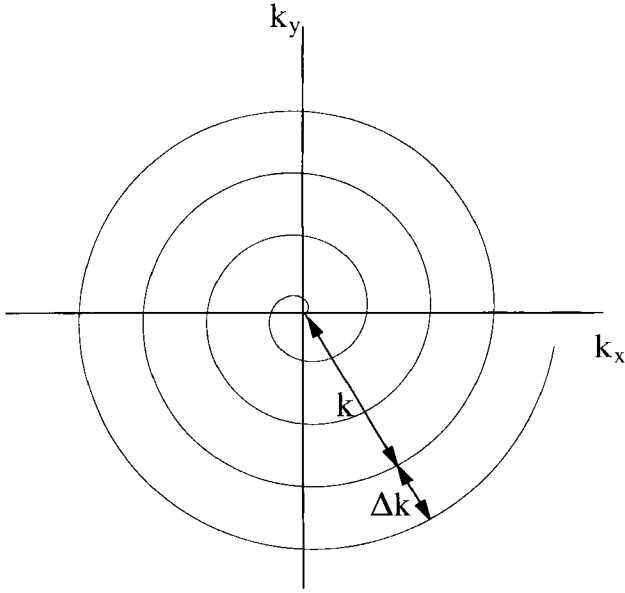


FIG. 1.  $k$ -Space trajectory of a single spiral interleaf showing radial sample spacing  $\Delta k$ .

number of interleaves (see Fig. 1). If the maximum  $\Delta k$  in Eq. [4] is chosen, Eq. [3] requires

$$A = \frac{M}{2\pi D}. \quad [5]$$

In the following section, we discuss how hardware constraints determine the gradient amplitude and slew rate, which are now calculated for later use. Using Eqs. [1]–[3], the Cartesian components of the gradient  $\mathbf{G}$  are given by

$$G_x = \frac{2\pi}{\gamma} \dot{k}_x = \frac{2\pi}{\gamma} A \dot{\theta} (\cos \theta - \theta \sin \theta), \quad [6]$$

$$G_y = \frac{2\pi}{\gamma} \dot{k}_y = \frac{2\pi}{\gamma} A \dot{\theta} (\sin \theta + \theta \cos \theta), \quad [7]$$

where a dot denotes the time derivative.

We define the instantaneous gradient slew rate  $\mathbf{S}$  as the time derivative of the gradient. Using Eqs. [6] and [7], the Cartesian components of  $\mathbf{S}$  are given by

$$S_x = \dot{G}_x = \frac{2\pi}{\gamma} A [(\ddot{\theta} - \theta \dot{\theta}^2) \cos \theta - (2\dot{\theta}^2 + \theta \ddot{\theta}) \sin \theta], \quad [8]$$

$$S_y = \dot{G}_y = \frac{2\pi}{\gamma} A [(\ddot{\theta} - \theta \dot{\theta}^2) \sin \theta + (2\dot{\theta}^2 + \theta \ddot{\theta}) \cos \theta]. \quad [9]$$

The vectors  $\mathbf{G}$  and  $\mathbf{S}$  rotate with time and have time varying magnitudes, denoted  $G$  and  $S$ , respectively, which we use later. Equations [6] through [9] can be used to show that  $G$  and  $S$  are given by

$$G = \frac{2\pi}{\gamma} A \dot{\theta} \sqrt{1 + \theta^2}, \quad [10]$$

and

$$S = \frac{2\pi}{\gamma} A [(\ddot{\theta} - \theta \dot{\theta}^2)^2 + (2\dot{\theta}^2 + \theta \ddot{\theta})^2]^{1/2}. \quad [11]$$

## HARDWARE CONSTRAINTS

We consider hardware constraints appropriate for the gradient amplifiers of a 1.5 T Signa scanner (GE Medical Systems, Milwaukee, WI). The constraints limit peak current, RMS current and slew rate. We consider only isotropic constraints where the limits are the same on all axes. Nonisotropic constraints can be handled by applying the most restrictive limits to all axes.

For a given  $k$ -space path, RMS current is reduced by increasing  $TR$ . The RMS current limit effectively becomes a limit on the minimum  $TR$ . Because our goal here is to minimize off-resonance blurring by minimizing readout time and not necessarily to minimize  $TR$ , we will not consider the RMS current limitation.

To derive the peak current and slew rate limitations, consider the LR circuit model for the gradient coil shown in Fig. 2. For a given axis, say  $x$ , the amplifier voltage  $V_x$  required to produce coil current  $I_x$  is given by

$$V_x = I_x R + L \frac{dI_x}{dt}, \quad [12]$$

where  $R$  and  $L$  are the resistance and inductance, respectively, of the gradient coil and are assumed to be the same for all three axes.

Equation [12] can be recast in terms of peak gradient slew rate and amplitude. Let the coil gain be  $g$ , defined by

$$G_x = I_x g, \quad [13]$$

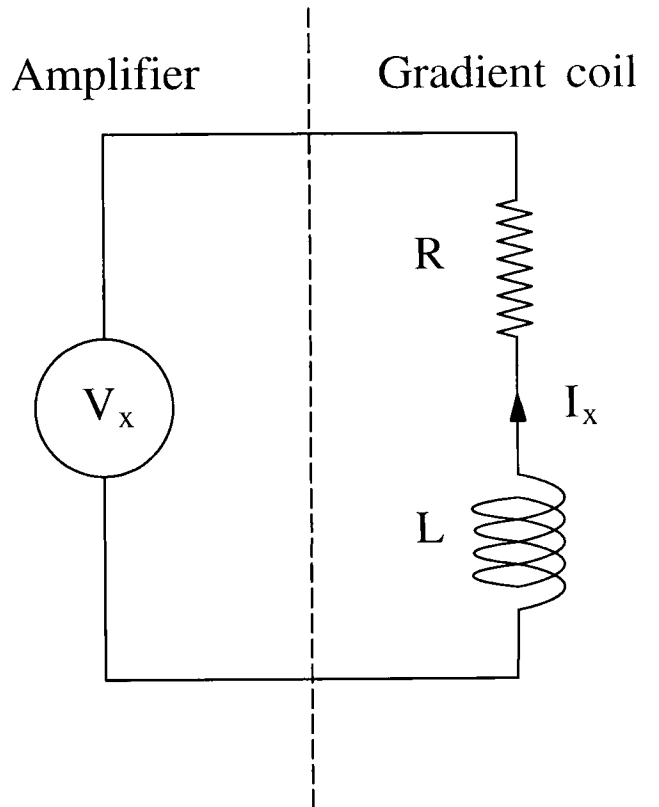


FIG. 2. Gradient coil equivalent LR circuit for the  $x$  axis. Amplifier voltage and coil current are  $V_x$  and  $I_x$ , respectively.

and let  $V_{\max}$  be the nominal maximum voltage obtainable from the gradient amplifier. Combining Eqs. [12] and [13] gives the gradient slew rate constraint

$$S_x \leq \frac{V_{\max}g - G_x R}{L}. \quad [14]$$

Let  $G_{\max}$  be the maximum gradient obtainable, where  $G_{\max}$  is determined from Eq. [13] by the peak instantaneous current and the coil gain  $g$ . The gradient slew rate limit in Eq. [14] is lowest when  $G_x = G_{\max}$ . We denote this most restrictive slew rate as  $S_{\max}$ , defined by

$$S_{\max} = \frac{V_{\max}g - R G_{\max}}{L}. \quad [15]$$

For fixed peak current, and coil characteristics determined by  $R$ ,  $L$ , and  $g$ ,  $S_{\max}$  is determined by the peak voltage  $V_{\max}$ . The peak instantaneous slew rate constraint for the  $x$  axis can then be described by

$$S_x \leq S_{\max} + \left(\frac{R}{L}\right)(G_{\max} - G_x). \quad [16]$$

The peak current constraint for the  $x$  axis can be described by

$$G_x \leq G_{\max}. \quad [17]$$

Constraints similar to Eqs. [16] and [17] hold for the other two axes.

### SPIRAL EQUATIONS OF MOTION

The least restrictive condition is to apply Eqs. [16] and [17] to the components of  $\mathbf{G}$  and  $\mathbf{S}$  on each axis. Instead we apply these equations to the magnitudes of the vectors, i.e., to  $G$  and  $S$ , as was done in refs. 1 and 12. The implications of this choice are discussed in the next section. We define

$$S_0 = S_{\max} + \left(\frac{R}{L}\right)(G_{\max} - G) \quad [18]$$

where, consistent with our assumption about isotropic constraints,  $R$  and  $L$  are defined to be the resistance and inductance for the axis with the smallest value of  $R/L$ . The optimized gradient solution is constrained by

$$S = S_0, \text{ if } G < G_{\max}, \quad [19]$$

$$\dot{G} = 0, \text{ otherwise.} \quad [20]$$

Equations [19] and [20] can be combined with Eqs. [10] and [11] to give the following differential equations for the spiral trajectory.

$$\ddot{\theta} = \frac{f(\theta, \dot{\theta}) - \theta \dot{\theta}^2}{1 + \theta^2}, \quad [21]$$

where

$$f(\theta, \dot{\theta}) = \begin{cases} [\alpha^2(1 + \theta^2) - \dot{\theta}^2(2 + \theta^2)]^{1/2} & \text{if } G < G_{\max}, \\ 0 & \text{otherwise} \end{cases} \quad [22]$$

and

$$\alpha = \frac{\gamma S_0}{2\pi A}. \quad [23]$$

Note that  $\alpha$  is implicitly a function of  $\theta$  and  $\dot{\theta}$  through the dependence of  $S_0$  on  $G$  in Eq. [18].

### RESULTS

Although we have not found analytical solutions to Eqs. [21] and [22], they can be solved by standard numerical methods. We have used regula falsa, and 4th order Runge-Kutta (16).

The benefit of using the circuit model is reduced readout time through faster increase of the gradient amplitude during readout. Not using the circuit model forces using the most restrictive slew rate in order to protect the hardware, i.e.,  $S_0 = S_{\max}$ . This result is equivalent to setting  $R/L = 0$  in Eq. [18]. We have analyzed the benefit of the circuit model by calculating the readout time for a single interleaf. The readout time was calculated by solving Eqs. [21] and [22] for  $\theta(t)$  and finding the value of  $t$  for which  $\theta(t) = k_m/A$  where  $k_m$  is the maximum spatial frequency required for the desired resolution. Figure 3 shows the  $x$  component of the  $k$ -space trajectory calculated with and without the circuit model, demonstrating that  $k_m$  is reached sooner when the circuit model is used. The circuit model approach is most beneficial for scan parameters for which the gradient amplitude does not

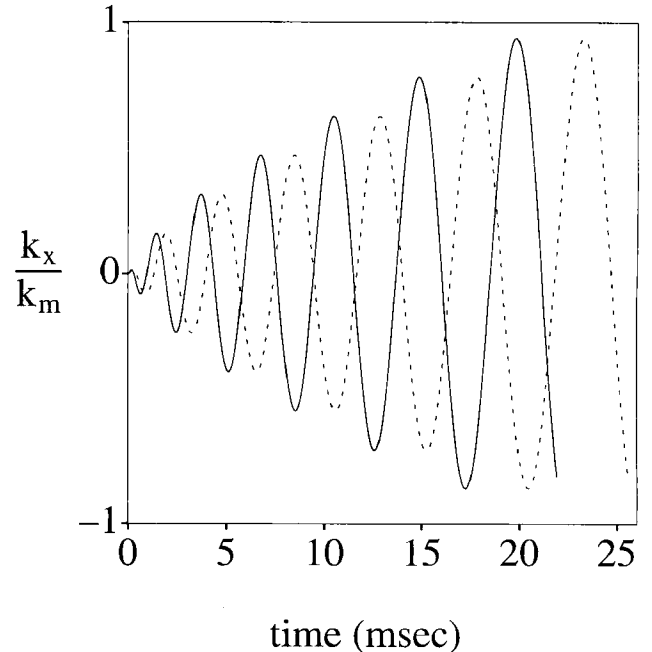


FIG. 3. Comparison of  $k_x/k_m$  as a function of time for gradient waveforms calculated with the circuit model (solid line,  $R/L = 1$  kHz) and without the circuit model (dashed line,  $R/L = 0$ ), where  $k_m$  is the maximum spatial frequency required. Acquisition parameters are 20 cm FOV, 20 interleaves, 256 pixels,  $S_{\max} = 17$  T/m/s and  $G_{\max} = 20$  mT/m. The values of  $G_{\max}$ ,  $S_{\max}$ , and  $R/L$  are hypothetical and not necessarily representative of actual performance for any commercial scanner.

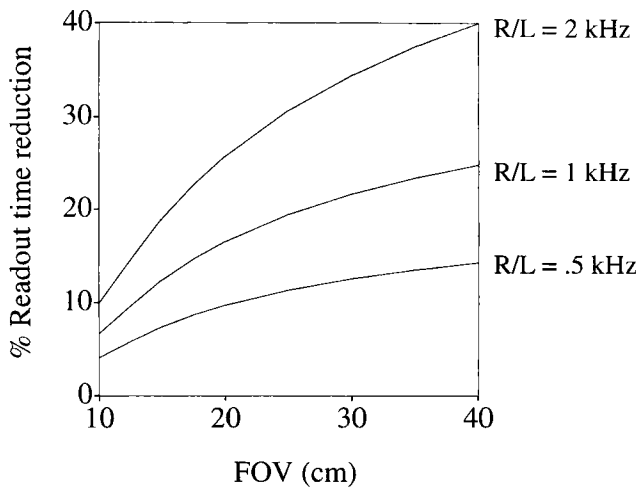


FIG. 4. Percentage reduction in readout time as a function of FOV using the circuit model for the following three values of  $R/L$ : 0.5, 1, and 2 kHz. Acquisition parameters are 20 interleaves, 256 pixels,  $S_{\max} = 17$  T/m/s and  $G_{\max} = 20$  mT/m.

reach  $G_{\max}$  by the time  $k_m$  is reached. For a fixed matrix size, increasing the FOV decreases  $k_m$ , decreasing the readout time, and decreasing the maximum gradient amplitude reached by the end of the readout. Thus, the readout time reduction from the circuit model increases with increasing FOV as shown in Fig. 4. The reduction was calculated by finding the percentage difference between the readout times for the values of  $R/L$  shown in the figure and the readout time for  $R/L = 0$ .

Figure 5 shows plots of the readout time for a single interleaf as a function of  $S_{\max}$ . For a fixed  $R/L$ , readout time decreases with increasing  $S_{\max}$  because the gradient reaches  $G_{\max}$  earlier in the acquisition. For  $S_{\max} \rightarrow \infty$ , the readout time approaches an asymptotic limit, independent of  $R/L$ , corresponding to  $G = G_{\max}$  for the entire scan. The benefit from the circuit model is reflected in the difference between the curve with  $R/L = 0$  and the other curves. This difference increases with decreasing

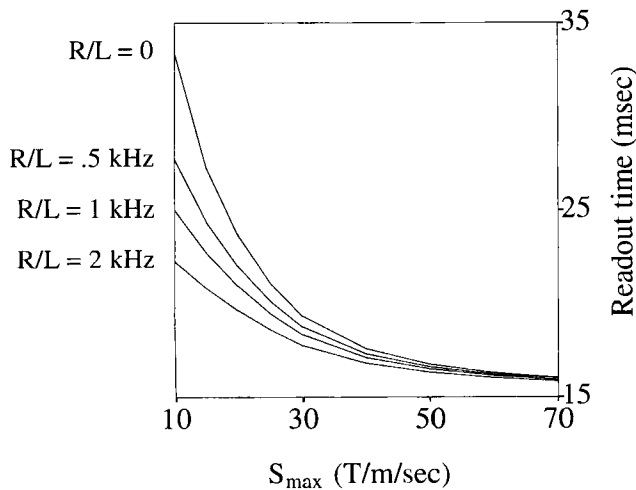
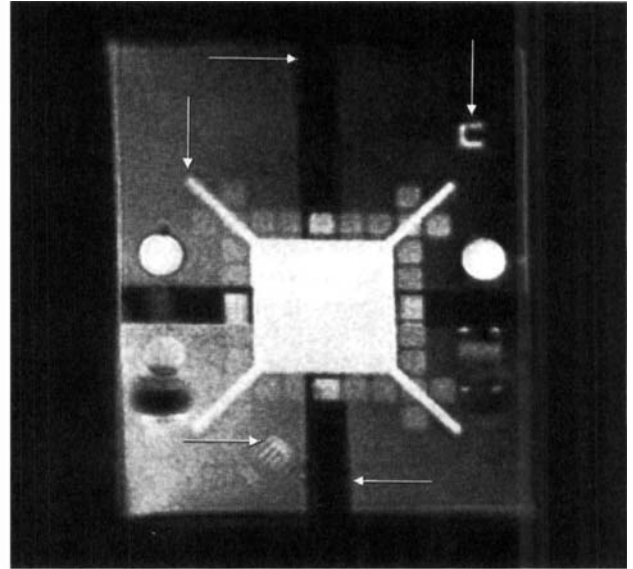


FIG. 5. Readout time for one interleaf as a function of  $S_{\max}$  for the following four values of  $R/L$ : 0, 0.5, 1, and 2 kHz. Acquisition parameters are 20 cm FOV, 20 interleaves, 256 pixels, and  $G_{\max} = 20$  mT/m.

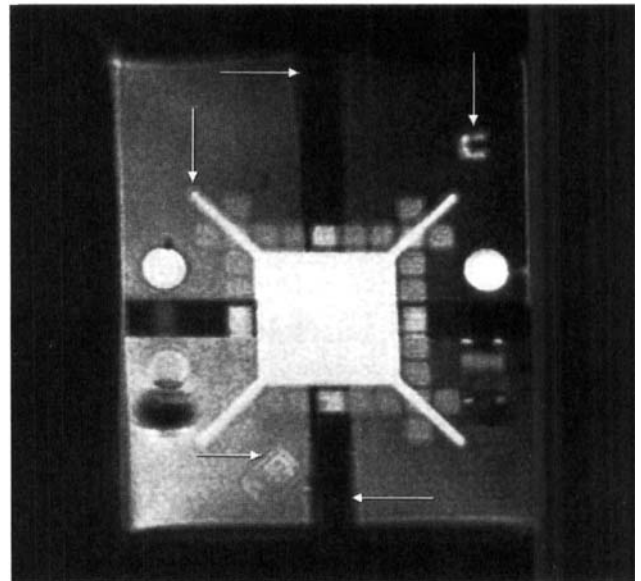
$S_{\max}$  because of the additional slew rate performance which the circuit model allows.

Figure 6 shows images of phantoms scanned using gradient waveforms calculated with and without the circuit model. Some areas where the blurring was reduced as a result of the circuit model are indicated with arrows.

For systems with small  $S_{\max}$ , corresponding to low peak voltage  $V_{\max}$ , the circuit model can be an effective method of improving performance in one of several



a



b

FIG. 6. Phantom scanned using gradient waveforms calculated (a) with the circuit model ( $R/L = 1$  kHz) and (b) without the circuit model ( $R/L = 0$ ). Acquisition parameters are 32 cm FOV, 14 interleaves, 256 pixels,  $S_{\max} = 20$  T/m/s and  $G_{\max} = 20$  mT/m. The circuit model reduced the readout time from 26.48 to 22.43 ms. Some areas where the blurring was reduced as a result of the circuit model are indicated with arrows.

ways. The readout can be shortened to reduce blurring as already discussed. Alternatively, the readout time and number of interleaves may be kept fixed, allowing greater  $k_m$  to be attained, with resulting higher resolution. Or the spatial resolution and readout time can be held fixed, and the number of interleaves decreased to reduce overall scan time.

Constraining the magnitudes of the rotating vectors  $\mathbf{G}$  and  $\mathbf{S}$ , instead of their components, guarantees that the hardware limits are not violated as the vectors are periodically aligned with the gradient axes, but is overly restrictive the rest of the time. This over-restriction has the advantage of simplifying calculation of gradient waveforms for multiple interleave scans. For multiple interleaves, the gradients may be calculated for one interleaf and waveforms for successive interleaves obtained by rotation. Constraining the magnitudes of the gradient and slew rate guarantees that the hardware limits are not violated for any rotation angle. We speculate that better performance results from a solution which applies Eqs. [16] and [17] to the components of  $\mathbf{G}$  and  $\mathbf{S}$  on each axis instead of to the vector magnitudes. An example of this approach for spiral gradients with 2D selective excitation is shown in (12).

## CONCLUSION

Off-resonance blurring in spiral scanning is minimized when the maximum gradient amplitude is used for the entire acquisition. When the maximum gradient amplitude approach is combined with constraints in the form of a circuit model for the gradient coil, the gradient waveforms for an Archimedean spiral are determined by a set of coupled differential equations. Solution of the equations shows that the readout is shorter when the circuit model is considered than when the most restrictive slew rate limit is imposed. For systems with limited slew rate capability, this approach can be effective at improving performance by reducing blurring, increasing spatial resolution or decreasing overall scan time.

## REFERENCES

1. C. H. Meyer, B. S. Hu, D. G. Nishimura, A. Macovski, Fast spiral coronary artery imaging. *Magn. Reson. Med.* **28**, 202–213 (1992).
2. C. H. Meyer, K. C. P. Li, J. M. Pauly, A. Macovski, Fast spiral  $T_2$ -weighted imaging, in "Proc., SMR, 2nd Annual Meeting, San Francisco, 1994," p. 467.
3. P. D. Gatehouse, D. N. Firmin, S. Collins, D. B. Longmore, Real time blood flow imaging by spiral scan phase velocity mapping. *Magn. Reson. Med.* **31**, 504–512 (1994).
4. A. T. Lee, G. H. Glover, C. H. Meyer, Discrimination of large venous vessels in time-course spiral BOLD MR functional neuroimaging, in "Proc., SMR, 2nd Annual Meeting, San Francisco, 1994," p. 652.
5. G. H. Glover, A. T. Lee, C. H. Meyer, Motion artifacts in fMRI: comparison of 2DFT with PR and spiral scan methods, in "Proc., SMRM, 12th Annual Meeting, New York, 1993," p. 197.
6. D. Nishimura, P. Irarrazabal, C. H. Meyer, A velocity  $k$ -space analysis of flow effects in echo-planar and spiral imaging. *Magn. Reson. Med.* **33**, 549–556 (1995).
7. E. Yudilevich, H. Stark, Spiral sampling in magnetic resonance imaging—the effect of inhomogeneities. *IEEE Trans. Med. Imaging* **MI-6**, 337–345 (1987).
8. D. C. Noll, C. H. Meyer, J. M. Pauly, D. G. Nishimura, A. Macovski, A homogeneity correction method for magnetic resonance imaging with time-varying gradients. *IEEE Trans. Med. Imaging* **10**, 629–637 (1991).
9. D. C. Noll, J. M. Pauly, C. H. Meyer, D. G. Nishimura, A. Macovski, Deblurring for non-2D Fourier transform magnetic resonance imaging. *Magn. Reson. Med.* **25**, 319–333 (1992).
10. P. Irarrazabal, D. Nishimura, Efficient  $k$ -space trajectories for fast three-dimensional imaging, in "Proc., SMR, 2nd Annual Meeting, San Francisco, 1994," p. 30.
11. C. B. Ahn, J. H. Kim, Z. H. Cho, High-speed spiral-scan echo planar NMR imaging-I. *IEEE Trans. Med. Imaging* **MI-5**, 2–7 (1986).
12. C. H. Hardy, H. E. Cline, Broadband nuclear magnetic resonance pulses with two-dimensional spatial selectivity. *J. Appl. Phys.* **66**, 1513–1516 (1989).
13. E. Yudilevich, H. Stark, Interpolation from samples on a linear spiral scan. *IEEE Trans. Med. Imaging* **MI-6**, 193–200 (1987).
14. J. D. O'Sullivan, A fast sinc function gridding algorithm for Fourier inversion in computer tomography. *IEEE Trans. Med. Imaging* **MI-4**, 200–207 (1985).
15. J. I. Jackson, C. H. Meyer, D. G. Nishimura, A. Macovski, Selection of a convolution function for Fourier inversion using gridding. *IEEE Trans. Med. Imaging* **10**, 473–478 (1991).
16. W. H. Press, S. A. Teukolsky, W. T. Vetterling, B. P. Flannery, "Numerical Recipes in C," Cambridge University Press, Cambridge, 1992.